[1.] Florentina BACIU, [2.] Mihai BUZATU, [3.] Florentina NICULESCU,
[3.] Gheorghe IACOB, [1.] Ion PENCEA

COMPARATIVE ANALYSIS OF DIFFERENT DENTAL IMPLANTS – PART II: EDS MAPPING OF THE ELEMENTAL DISTRIBUTIONS

[1.] Doctoral School of the Materials Science and Engineering Faculty, National Scientific and Technological POLITEHNICA University of Bucharest, Bucharest, ROMANIA
[2.] University of Medicine and Pharmacy "Carol Davila" Bucharest", Bucharest, ROMANIA
[3.] Materials Science and Engineering Faculty, National Scientific and Technological POLITEHNICA University of Bucharest, Bucharest, ROMANIA

Abstract: In this paper, three types of dental alloys often used in practice were investigated, namely: NiCrMoSiVCuFe, NiCrMoSiFeAlMgZn and CuAlNiFeMgZnSi to evaluate the chemical homogeneity. Energy Dispersive X–ray Spectroscopy (EDS) and Backscattered–Electron (BSE) Imaging were used to obtain valid results on the structure and distribution of constituent elements in the investigated alloys. All samples were investigated in 3 different (micron) areas, respectively: a central area and two marginal areas. The EDS investigations followed the identification of the spectral lines, respectively the irrefutable highlighting of the composition of the sample and, subsequently, the distributions of the identified elements in the specified areas to be compared. The mapping distributions of the elements can reveal local homogeneity/heterogeneity (in bottle heterogeneity) and homogeneity at the sample (implant) level (between bottles heterogeneity). The microstructural inhomogeneity resulting from the formation of compounds in the grain boundaries is primary and determines, therefore, elemental or chemical heterogeneity.
Keywords: biomedical alloys, dental implants, homogeneity, microstructure, elemental distribution

1. INTRODUCTION

Nickel–based alloys are materials primarily composed of nickel with other elements added to enhance mechanical, thermal, and corrosion–resistant properties. These alloys are widely used in industries requiring high performance in extreme conditions, such as aerospace, chemical, and energy sectors. Due to the presence of elements like chromium and molybdenum, nickel–based alloys exhibit exceptional corrosion resistance in various chemical environments and at high temperatures [1]. Nickel imparts excellent high–temperature stability, maintaining macanichal strength and hardness. These alloys possess a combination of mechanical and chemical properties, making them ideal for use in extreme conditions where other materials would fail. Surgical instruments and medical equipment are made from nickel–based alloys due to their biocompatibility and corrosion resistance. Nickel–based alloys continue to be developed and optimized to meet the increasingly demanding requirements of modern industry, being essential for technological advancements in many fields [2, 3].

Copper–based alloys are widely used in the medical field due to their antibacterial properties, biocompatibility, and corrosion resistance. Copper and its alloys can destroy a wide range of microorganisms, including bacteria, viruses, and fungi, which is essential for preventing nosocomial infections (hospital–acquired infections) [4]. Copper alloys are used in stents and heart valves due to their corrosion resistance and ability to inhibit the development of bacterial biofilms [5]. Copper nanoparticles are being researched for antibacterial treatments due to their enhanced efficiency in combating bacteria at the nanoscale [6. Medical alloys based on copper (Cu), aluminum (Al), and nickel (Ni) are used for their unique combination of mechanical properties and biocompatibility. These materials are essential in various medical applications, such as surgical instruments, implantable devices, and medical equipment [3, 7]. Specific applications of these alloys include the manufacture of prostheses and implants, surgical instruments, and medical imaging devices. These alloys are used for prostheses and implants due to their biocompatibility and durability [8]. For example, Al–Ni alloys are used for dental and orthopedic implants. Cu–Ni and Al–Cu–Ni alloys are used for making surgical instruments due to their corrosion and wear resistance, as well as ease of sterilization. Due to their electromagnetic properties, copper–nickel alloys are used in components of imaging devices, such as MRI machines [9].

Copper, aluminum, and nickel–based alloys represent an essential part of modern medical technology, contributing to improving the quality of life for patients through their performance and reliability in various medical applications [4, 6, 10, 11]. Advantages of these types of alloys include excellent corrosion resistance in biological environments, biocompatibility, minimizing the risk of adverse reactions, adaptable mechanical properties for various medical applications, and ease of processing and forming

ISSN 1584 – 2665 (printed version); ISSN 2601 – 2332 (online); ISSN-L 1584 – 2665

into complex shapes [4, 5, 10, 12]. Main disadvantages of the previously mentioned alloys are related to relatively high production costs, the need for strict quality control processes to ensure biocompatibility and material performance [4, 13, 14].

2. MATERIALS AND METHODS

To evaluate the chemical homogeneity of the samples, they were investigated using Energy Dispersive X–ray Spectroscopy (EDS) and Backscattered–Electron (BSE) Imaging. EDS is an analytical technique used for elemental analysis or chemical characterization of a sample. This is based on the punctual interaction between an incident electron beam and the atoms of the material, respectively characteristic lines of X–rays specific to each element are generated through electronic transitions induced by the electron beam [15]. When a material is bombarded with a concentrated beam of electrons (Scanning Electron Microscopy – SEM, or Transmission Electron Microscope – TEM), electrons from the inner shells of the atoms in the material are ejected, creating electron vacancies. These vacancies are filled by electrons from higher energy levels, and the energy difference is released by emission of a X–ray photon. The energy of this photon is characteristic of the element from which it was emitted. An EDS detector measures the energy and intensity of these emitted X photons. The energy of the X photon identifies the element (qualitative analysis), and the intensity X–ray spectral line associated with the element is used to estimate the concentration of the element (quantitative analysis). Quantification of the elemental composition of the sample from the target micron volume is performed based on the intensities of the spectral lines of the elements that form the spectrum, using calculation programs that assist both the operation of the spectrometer and the elaboration of test reports [16].

EDS spectrometry, which is implemented as auxiliary equipment of SEM microscopes, has 3 modes of operation: 1) spot; 2) linear and 3) areolar (mapping). In point mode, EDS provides a spectrum of characteristic lines related to a volume of about 1 μm^3 centered on the targeted point. In linear mode, EDS provides the values of the concentrations of an element along a right segment and in mapping mode, EDS provides an estimate of the concentrations of an element within a perimeter/target area. In all cases, the information regarding the elemental concentrations refers to the superficial layer of the sample, which has a thickness of 2–10 μm.

BSEs are high–energy electrons used to obtain high–resolution images that show the distribution of various elements that make up a sample. By having a clear understanding of how BSEs work we can obtain the high–quality images needed to advance the research.

Table 1. The types of alloys investigated

Sample code	Alloy type
Sample 1	NiCrMoSiVCuFe
Sample 2	NiCrMoSiFeAlMgZn
Sample 3	CuAlNiFeMgZnSi

Three types of samples were analyzed, as it is shown in Table 1. Before the investigations, the samples were thoroughly metallographically prepared due to their complex geometries. The microstructural analysis was performed using the EBSD technique, using a TESCAN VEGA II—XMU scanning electron microscope (SEM) provided with a BRUKER eFlash1000 EBSD detector, and also through this device the chemical compositions of the studied alloys were determined.

All samples were investigated in 3 different (micron) areas, respectively: a central area and two marginal areas. The EDS investigations followed the identification of the spectral lines, respectively the irrefutable highlighting of the composition of the sample and, subsequently, the distributions of the identified elements in the specified areas to be compared. The mapping distributions of the elements can reveal local homogeneity/heterogeneity (in bottle heterogeneity) and homogeneity at the sample (implant) level (between bottles heterogeneity).

3. RESULTS AND DISCUSSION

The results of the SEM–EDS investigations consist of BSDE (Backscatter Electron Diffraction) images and images (mappings) of the elemental compositions of the main elements of the studied alloy. The EBSD mode of microscopy facilitates the observation of individual grain orientations, local texture and the identification of phase distributions on the surfaces of polycrystalline materials [17]. Three representative positions were selected, i.e. in the center, inner edge, and outer edge. Figures 1–9 show the results obtained for the three representative samples depending on the location chosen for the investigation. The EDS spectrum obtained on the inner edge area of Sample 1 (Figure 1) shows all the

ISSN 1584 – 2665 (printed version); ISSN 2601 – 2332 (online); ISSN-L 1584 – 2665

spectral lines specific to the NiCrMoSiVCuFe alloy, well defined. The respective spectrum has an adequate radiation background that facilitates a sensitive elemental analysis.

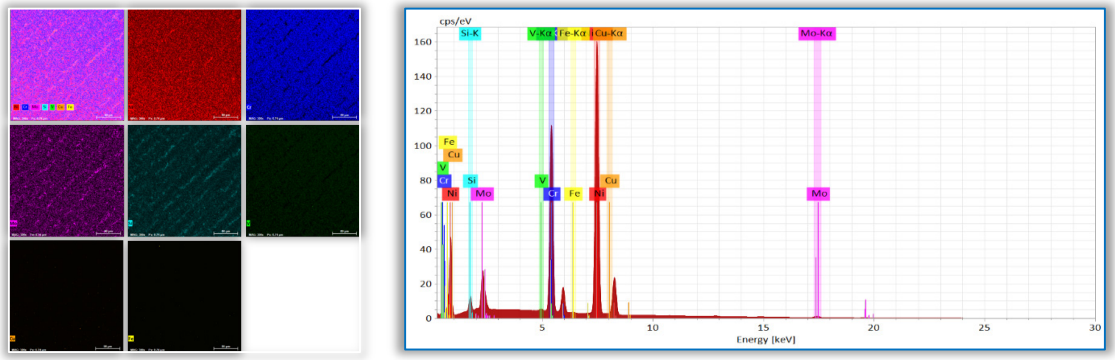

Figure 1. BSED images and EDS analysis for the inner edge of Sample 1 showing the distribution of elements Ni, Cr, Mo, Si, V, Cu and Fe in the respective area

The microstructure of the "inner edge Sample 1" area has a reticular appearance with rows of compounds located at distances of 10–15 μm. The compounds highlighted by lighter colored areas are richer in Ni, Mo and Si than the surrounding areas. They are poorer in Cr, V and Mg. Figure 1 shows that the elements Ni, Cr, Mo and Si are unevenly distributed in the respective area, while the elements V, Cu, Fe and Mg are uniformly distributed. The elemental inhomogeneities are caused by the precipitation of compounds, most likely at the grain boundaries.

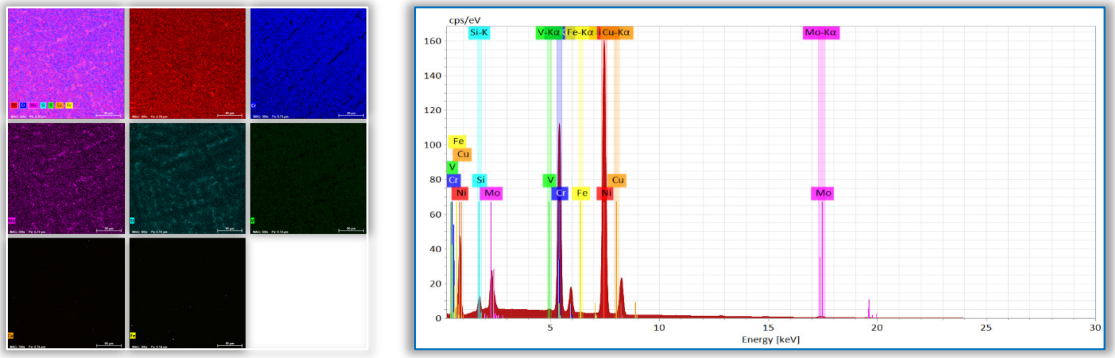

Figure 2. BSED images and EDS analysis for the center of Sample 1 showing the distribution of elements Ni, Cr, Mo, Si, V, Cu and Fe in the respective area

The characteristic lines of Ni, Cr and Si from the EDS spectrum obtained on the central area of Sample 1 are well defined and intense in the EDS spectrum from Figure 1, while the lines of elements V, Cu and Fe are doubtful. The EDS spectrum in Figure 2 also has a low radiative background similar to the EDS spectra presented previously.

The microstructure of the central area of Sample 1 has the same composite appearance as the microstructure of the "inner edge of Sample 1" area. The lighter colored phase contains in larger quantities the elements Ni, Mo and Si compared to the adjacent phase. The lighter colored phase contains less Cr. It is observed that the distribution of Cr has a reticular symmetry centered on inclined segments where there are portions with a lack of Cr. Mo and Si also present distributions with a reticular appearance indicating a precipitate of compounds, most likely at the grain boundaries. And this sample shows elemental heterogeneity that is combined with a microstructural heterogeneity generated, most likely, in the solidification process of the alloy (implant) which involves segregation of Si, Mo and Cr elements. Cr behaves differently, in the sense of reverse diffusion.

The EDS spectrum presented in Figure 3 and obtained on the area of the outer edge of Sample 1 is quasi–identical with the spectra presented previously i.e. it shows all the spectral lines specific to the NiCrMoSiVCuFe alloy. And in this case, the Ni line is better defined than in the case of Figure 1. The EDS spectrum in Figure 3 has a low radiation background similar to the EDS spectra presented previously.

The microstructure of the outer edge of sample 2 is well revealed by the BSDE–SEM image which shows a square cell microstructure delimited by compounds aligned in mutually orthogonal rows. The respective compounds, which are highlighted by a lighter color, are composed of Ni, Mo and Si. V, Cu

ISSN 1584 – 2665 (printed version); ISSN 2601 – 2332 (online); ISSN-L 1584 – 2665

and Fe are uniformly distributed in the investigated area, while Cr shows textured areas where it seems to be missing i.e. shows reverse diffusion.

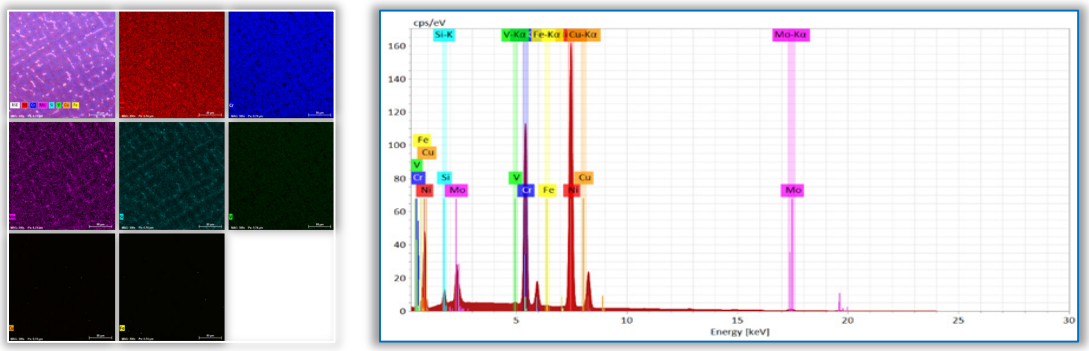

Figure 3. BSED images and EDS analysis for the outer edge of Sample 1 showing the distribution of elements Ni, Cr, Mo, Si, V, Cu and Fe in the respective area

This area also presents elemental heterogeneity that combines with a microstructural heterogeneity generated, most likely, in the process of cellular solidification of the implant in the mold. The marginal area had a more pronounced heat transfer, which can explain its microstructure and implicitly the segregation of Si, Mo and Cr elements. And in this case, Cr behaves differently, in the sense of reverse diffusion.

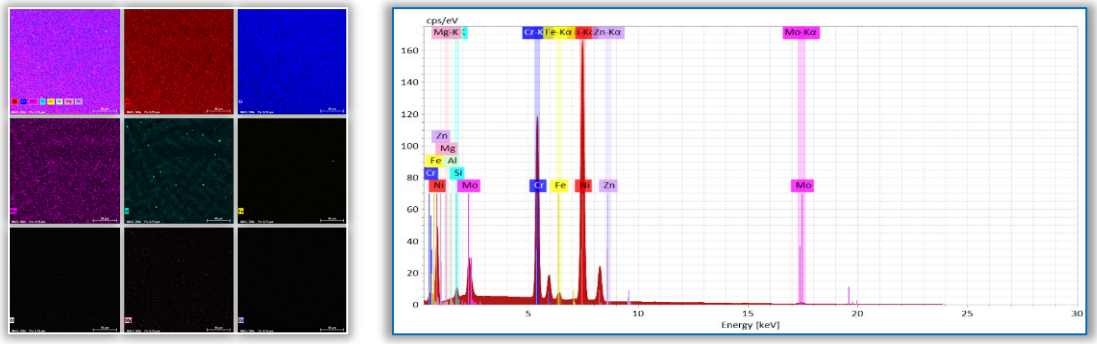

Figure 4. BSED images and EDS analysis for the inner edge of Sample 2 showing the distribution of elements Ni, Cr, Mo, Si, Fe, Al, Mg and Zn in the respective area

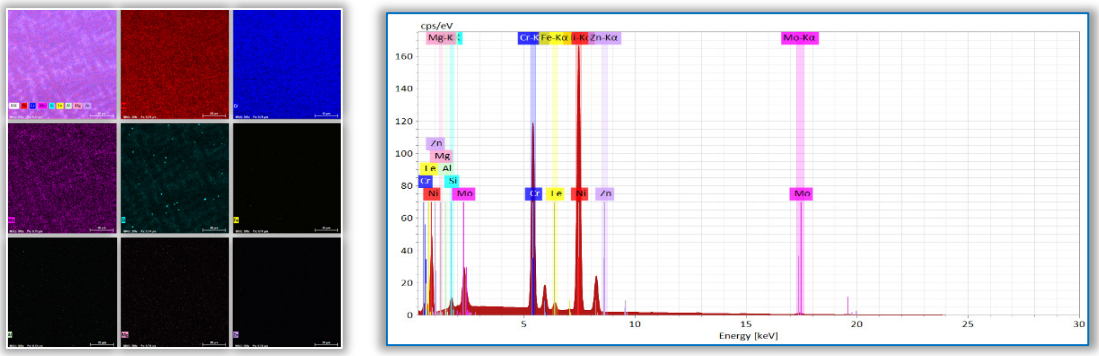

Figure 5. BSED images and EDS analysis for the center of Sample 2 showing the distribution of elements Ni, Cr, Mo, Si, Fe, Al, Mg and Zn in the respective area

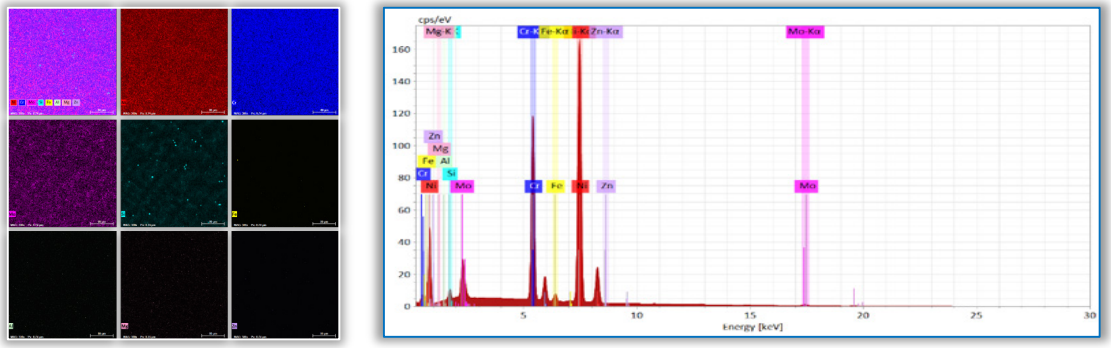

Figure 6. BSED images and EDS analysis for the outer edge of Sample 2 showing the distribution of elements Ni, Cr, Mo, Si, Fe, Al, Mg and Zn in the respective area

ISSN 1584 – 2665 (printed version); ISSN 2601 – 2332 (online); ISSN-L 1584 – 2665

The EDS spectra obtained on the inner edge, center and outer edge areas of Sample 2 (Figures 4–6) show all the spectral lines specific to the NiCrMoSiFeAlMgZn alloy, well defined. The respective spectra have an adequate radiation background that facilitates a sensitive elemental analysis.

The microstructural aspects are similar between Samples 1 and 2, and in this case, there is an entanglement of phases, most likely α and γ. To establish the nature of the phases in the BSED image, new EDS and electron diffraction investigations are required

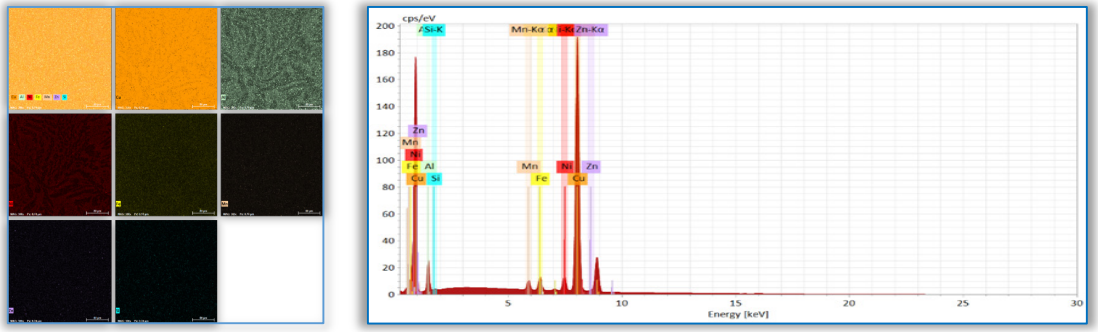

Figure 7. BSED images and EDS analysis for the inner edge of Sample 3 showing the distribution of elements Cu, Al, Ni, Fe, Mg, Zn and Si in the respective area

The EDS spectrum presented in Figure 7 shows the characteristic lines of the elements Cu, Al, Ni, Fe, Mg and Zn which were expected for the alloyed aluminum bronze, i.e. CuAl9Ni3Fe2Mg2Zn0.7Si0.2. The lines of the elements Cu, Ni, Mn and Fe are relatively intense and well defined, while the lines of the elements Al, Si and Zn have low intensities at the background level and overlap with other spectral lines. The radiative background of the EDS spectrum in Figure 7 is low which allows an adequate deconvolution of the spectral lines.

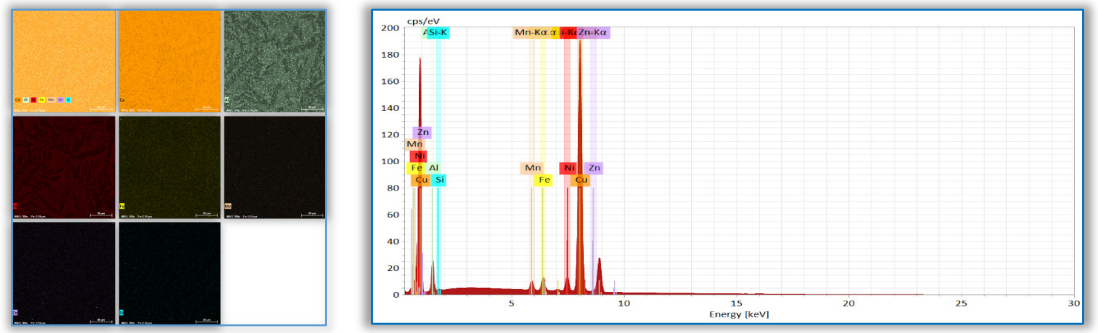

Figure 8. BSED images and EDS analysis for the center of Sample 3 showing the distribution of elements Cu, Al, Ni, Fe, Mg, Zn and Si in the respective area

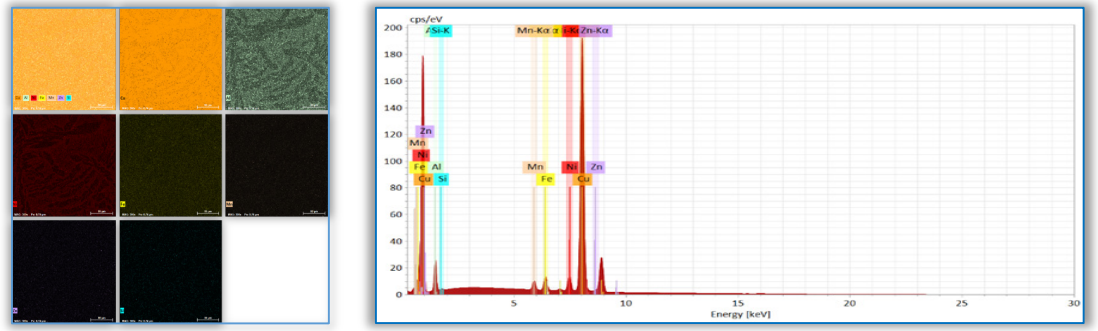

Figure 9. BSED images and EDS analysis for the outer edge of Sample 3 showing the distribution of elements Cu, Al, Ni, Fe, Mg, Zn and Si in the respective area

The microstructure of the inner edge of Sample 3 revealed by the BSDE–SEM image is monophasic (α phase). Submicron compounds rich in Al can be observed in the alloy matrix. Also, the mappings of Cu, Al and Ni elements indicate a textural correlation that can be attributed to an entanglement of α and γ phases resulting from the decomposition of the β phase [18].

The elements Fe, Mn, Zn and Si are uniformly distributed in the investigated area. Elemental heterogeneities are manifested in the cases of Al and Ni, which also implies a heterogeneity of Cu. For the parsimonious estimation of the elemental heterogeneity in correlation with the microstructural heterogeneity, comprehensive experiments are required.

ISSN 1584 – 2665 (printed version); ISSN 2601 – 2332 (online); ISSN-L 1584 – 2665

The EDS spectrum, the microstructure and the distribution of the elements in the center area of Sample 3 show the same characteristics as in the case of the "inner edge of Sample 3" area. There is an entanglement of phases, most likely α and γ. To establish the nature of the phases in the BSED image, new EDS and electron diffraction investigations are required.

The information provided by Figure 9 attests that the "outer edge Sample 3" area presents the same microstructural aspects as the elemental distributions as those provided by the BSED–EDS investigations in the inner and central edge areas of the implant made of cast aluminum bronze.

4. CONCLUSIONS

The implants made of the NiCrMoSiVCuFe superalloy present "in bottle" and "between bottle" type heterogeneities both at the elemental distribution level and at the microstructural level. In this study, it is considered that the microstructural inhomogeneity resulting from the formation of compounds in the grain boundaries is primary and determines, as a consequence, elemental or chemical heterogeneity.

Cr has a special behavior in the sense that it undergoes reverse diffusion, i.e. diffuses to the interior of the grain. It is known that Cr tends to diffuse selectively in the grain boundary in the case of Ni–based superalloys.

The explant made from the CuAl9Ni3Fe2Mg2Zn0.7Si0.2 alloy, which can be considered as a CuAl6T type bronze, shows an advanced microstructural uniformity both locally (in bottle) and globally (between bottles). In the matrix of the alloy there are submicron compounds rich in uniformly distributed Al.

Although it was expected that the explant made of CuAl9Ni3Fe2Mg2Zn0.7Si0.2 would be monophasic (α phase), it was proven that it is biphasic, most likely the α and γ phases which may result from the decomposition of the β phase in the type of implant cooling.

The results presented in this work open new perspectives regarding the performance of more detailed research that will clearly highlight the microstructural and compositional aspects that will lead to a pertinent and exhaustive evaluation of the material and subsequently contribute to the improvement of the functionalization of the implants.

References

[1] Haider A., Azam O., Talha M., Akhtar S. Ni–Cr–Mo Alloy for Dental Prostheses with Low Melting Temperature, Key Engineering Materials, 2018, 778, pp. 301–305.
[2] Muller A.W.J. Corrosion of dental NiCrMo alloys, Thesis, 1990.
[3] Kumar M.P. Manikandan M. Investigation of corrosion behaviour on Ni–Cr–Co and Ni–Cr–Mo alloys exposed to molten salt for thermal energy storage applications, Corrosion Engineering, Science and Technology, 2023, 58(1), pp. 49–60.
[4] Niinomi M. Co–Cr–based alloys Structural Biomaterials Properties, Characteristics and Selection, Woodhead Publishing Series in Biomaterials, 2021, pp. 103–126.
[5] Qi J., Ma L., Gong P., Rainforth W.M. Investigation of the wear transition in CoCrMo alloys after heat treatment to produce an HCP structure, Wear, 2023, 518–519, art. no. 204649.
[6] Gvk, S.S. Co–Cr–Ni–Mo wires for medical applications: processing, mechanical, microstructure and fatigue characterization, Doctoral thesis, 2019, Nanyang Technological University, Singapore.
[7] Abolhasani D, Han S.W., VanTyne C.J., Kang Na., Moon Y.H. Enhancing the shape memory effect of Cu–Al–Ni alloys via partial reinforcement by alumina through selective laser melting, J. Mater. Res. Technol., 2021, 15, pp. 4032–4047.
[8] Gojics M., Kozuh, S., Ivan A., Lojen G. Ivanic I. Kosec B., Microstructural and phase analysis of CuAlNi shape–memory alloy after continuous casting, Materials and Technologies, 2013, 47(2), pp. 149–152.
[9] Pan W., Ye Z., Zhang Y., Liu Y., Liang B., Zhai Z. Research on Microstructure and Properties of AlSi10Mg Fabricated by Selective Laser Melting, Materials, 2022, 15(7), art. no. 2528.
[10] Haider A., Jaffery S.H.I., Khan A.N., Qadir N., Jing X. Effect of cerium on mechanical, metallurgical and biomedical properties of NiCrMoB dental alloy, J. Mater. Res. Technol., 24, pp. 5082–5093.
[11] Buzatu M., Geantă V., Ştefănoiu R., Buţu M., Petrescu M.I., Buzatu M., Ghica V.G., Niculescu F., Iacob G. Influence of the Tungsten Content on the Elastic Modulus of New Ti–15Mo–W Alloys Intended for Medical Applications, JOM, 2019, 71(7) pp. 2272–2279.
[12] Buzatu M, Petrescu M.I., Geantă V., Ştefănoiu R., Buzatu M., Buţu M., Iacob G., Niculescu F. Full factorial design for Ti–Mo–W beta alloys to correlate the modulus of elasticity with the material parameters Md, Bo and e/a, U.P.B. Sci. Bull., Series B, 2022, 84(4), pp. 181–190.
[13] Yang K.R., Hanawa T. Kwon T.Y., Min B.K., Hong M.H. Mechanical Property Comparison of Ni–Cr–Mo Alloys Fabricated via One Conventional and Two New Digital Manufacturing Techniques, Appl. Sci., 2021, 11(19), 9308.
[14] Jo M.G., Ryu S.H., Kim K.I., Kim D.E., Kim J.I., Kim K.T., Kim S.S., Cho G.S., A Study on the Microstructures and Mechanical Properties of Ni–Cr–Mo–V Low Alloy Steels, Korean J. Met. Mater., 2022, 60(4), pp. 251–262.
[15] Pencea I. Instrumental methods and techniques for elemental analysis of materials, chapter 8, in Treatise on Materials Science and Engineering, vol. 5, entitled: Final processing technologies of metallic materials, Agir Publishing House, 2011, pp. 1057–1239, (in Romanian).
[16] Rousseau R.M., Detection limit and estimate of uncertainty of analytical XRF results, The Rigaku Journal, 2001, 18(2), pp. 33–47.
[17] Humphreys F.J., Brough I. High resolution electron backscatter diffraction with a field emission gun scanning electron microscope, J Microsc., 1999, 195(1) pp. 6–9.
[18] Popescu N., Şaban R., Bunea D., Pencea I. Ştiința materialelor pentru ingineria mecanica – alcătuirea, generarea şi comportarea structurii materialelor metalice. Aliaje fier – carbon, Ed. Fair Partners, Bucharest, 1999.

ISSN 1584 – 2665 (printed version); ISSN 2601 – 2332 (online); ISSN-L 1584 – 2665